Rapid Communications

Redox-controlled epitaxy and magnetism of oxide heterointerfaces: $EuO/SrTiO_3$

Patrick Lömker[1,2] and Martina Müller[2,3,*]

[1]*Photon Science, Deutsches Elektronen Synchrotron, D-22607 Hamburg, Germany*

[2]*Peter Grünberg Institut (PGI-6), Forschungszentrum Jülich GmbH, D-52428 Jülich, Germany*

[3]*Fakultät Physik, Technische Universität Dortmund, D-44221 Dortmund, Germany*

(Received 13 February 2019; revised manuscript received 26 April 2019; published 20 June 2019)

We demonstrate a route to prepare thin films of the ferromagnetic insulator europium monoxide. Key is a redox-controlled interface reaction between metallic Eu and the substrate $SrTiO_3$ as the supplier of oxygen. The process allows tuning the electronic, magnetic, and structural properties of the EuO films. Furthermore, we apply this technique to various oxidic substrates and demonstrate the universality and limits of a redox-controlled EuO film synthesis.

DOI: 10.1103/PhysRevMaterials.3.061401

I. INTRODUCTION

Oxidic thin films, multilayers, or heterostructures are becoming increasingly important in a wide range of cutting-edge applications [1]. This includes novel field-effect transistors, spin-, magneto-, and orbitronics, as well as topological oxide electronics [2–5]. Among the class of magnetic oxides, the ferromagnetic insulator europium monoxide (EuO) represents one of the most intriguing functional materials, as it combines strong local $4f^7$ ferromagnetism with electrical insulation [6,7]. In that, EuO offers the opportunity to probe quantum phenomena [8] and can serve as a building block for a multitude of future spin-based applications such as magnetically gated two-dimensional electron systems with potential application of the inverse Edelstein effect [9–13].

Oxide synthesis with atomic layer precision requires large experimental efforts; simultaneously varying the oxide properties introduces a further challenge. In the particular case of EuO, the adsorption-limited growth mode has become the standard approach for thin film growth [14]. This process is limited in two ways as it can only be applied to inert substrates and determining the appropriate deposition parameters is a complex task [15]. The three parameters substrate temperature, oxygen gas, and metal fluxes must be controlled simultaneously.

The idea of the adsorption-limited growth process is to avoid overoxidation of (metastable but ferromagnetic) EuO into (stable but paramagnetic) Eu_3O_4 and Eu_2O_3. This is achieved by adjusting the flux ratio to Eu rich and taking advantage of the temperature-dependent reevaporation, or "distillation," of excess Eu metal [16,17].

In view of this laborious process, alternative growth schemes aim at simplifying experimental procedures. For instance, in a so-called "topotactic" growth mode, Eu_2O_3 is capped by a Ti metal top layer, which causes the oxidation of Ti to TiO_2 and the reduction of Eu_2O_3 to stoichiometric EuO [18]. The resulting EuO thickness was restricted to a few nanometers. This procedure limits the choice of overlayer material to titanium and also requires a careful tuning of the Eu_2O_3/Ti bilayer thickness for its complete reduction/oxidation. Moreover, the resulting TiO_2 overlayer, a wide-band insulator, prevents the universal integration of EuO into functional heterostructures and transport devices.

For the growth of EuO thin films and heterostructures, the substrate itself is usually not considered as an active part of the oxide growth process. However, most oxidic substrates *do not* act as "passive" templates. Instead, they can cause undesirable changes in the properties of the overlayer, e.g., by oxygen ion diffusion. To avoid chemical interactions on "active" substrates a buffer layer is often applied in between substrate and film. Particular to EuO, previous reports found that adsorption-limited synthesis directly on $SrTiO_3$ is not possible. The deposition of EuO is made possible by the application of a SrO or BaO buffer layer [19,20]. The thermodynamics at the interface play an important role on the stoichiometry of the grown film [15].

In this work, we present a conceptionally reverse approach. A redox reaction between a metallic reactant, Eu, and an oxidic substrate, $SrTiO_3(001)$, determines the stoichiometry of the growing Eu-oxide overlayer—without supplying gaseous oxygen during synthesis. The temperature dependence of the conductivity for ionic oxygen is used to control both the final thickness and the stoichiometry of the redox-grown EuO film.

Our route for EuO synthesis allows one to carefully control the chemical, magnetic, and structural properties of the Eu oxides and thereby enhances the possibilities of oxide heterostructure preparation by a simple, effective bottom-up approach. Contrary to results, where substrate-related oxygen transfer is negligible [17], we apply this technique to various oxidic substrates and demonstrate the universality of this redox-controlled EuO film synthesis. We believe the technique can be easily generalized to the design of other functional oxides thin films, interfaces, and heterostructures.

II. EXPERIMENTAL DETAILS

For the investigation of the redox growth of EuO on $SrTiO_3(001)$ without additional oxygen gas we have

*mart.mueller@fz-juelich.de

developed a stepwise deposition method. As substrate we employed Nb:$SrTiO_3$(001) and pure Eu metal was evaporated from a Knudsen cell in an ultrahigh-vacuum molecular beam epitaxy system. Further details are given in the Supplemental Material [21]. Deposition steps of pure Eu metal alternate with *in situ* structure analysis [reflection high-energy electron diffraction (RHEED), and low-energy electron diffraction (LEED)] and chemical analysis [x-ray photoelectron spectroscopy (XPS)]. The stepwise deposition was carried out such that the total deposition time was stopped to enable analysis at the times $t = (1, 2, 5, 10, 20,$ and $60)$ min. Between two deposition steps, the sample is cooled from T_P to room temperature for analysis. This procedure is repeated for different substrate temperatures. In this way, a chemical and structural growth profile of europium oxide on $SrTiO_3$ is obtained depending on the deposition time t and temperature T_P as determined from the pyrometer (see [21]).

In situ XPS is conducted on Ti $2p$ and Eu $3d$ core levels with a PHOIBOS-100 hemispherical energy analyzer using Al $K\alpha$ radiation from an x-ray anode (SPECS).

We characterize the structure *ex situ* with x-ray diffraction (XRD), x-ray reflection (XRR), and reciprocal space mapping (RSM). Magnetic properties are analyzed with vibrating sample magnetometry and a magnetic property measurement system (see Supplemental Material [21]).

III. RESULTS

Our study combines the redox-driven EuO synthesis with a chemical and structural *in situ* (XPS, LEED, RHEED) and magnetic and structural *ex situ* (SQUID, XRD, XRR, RSM) analysis.

First, we acquire reference spectra of the Eu $3d_{5/2}$ core level [Fig. 1(a)] as a function of the valence of the Eu cations. As reference systems, we prepare films of pure phases ($d =$ 10 nm) of Eu^0 (Eu metal), Eu^{2+} (EuO), and Eu^{3+} (Eu_2O_3; see Supplemental Material [21]). The Eu $3d_{5/2}$ peak of divalent Eu^{2+} is located at $E_B = 1125$ eV [15,22,23]. This peak is accompanied by a satellite peak (S) at higher binding energy, which is part of the multiplet of the $3d^9\,4f^7$ final state [23]. Eu metal is observed at the same binding energy. In order to clearly distinguish the reference spectra of metallic Eu from the divalent state, we use the Doniach-Sunjic inelastic background, which is only present in metallic samples. At $E_B = 1135$ eV the Eu $3d_{5/2}$ peak is detected for trivalent Eu^{3+}. At $E_B = 1125$ eV an x-ray satellite from the trivalent Eu $3d_{5/2}$ is observed as a consequence of using nonmonochromatized Al x rays.

The sensitivity of the Doniach-Sunjic background shape as a measure for metallic Eu^0 is demonstrated by comparing a stoichiometric EuO film on yttria-stabilized zirconia [YSZ(001)] with $d \approx 2$ Å Eu metal deposited on a Cu(001) single crystal. The Doniach-Sunjic inelastic background for this sample is clearly observed [Fig. 1(b)], showing that even monolayers of Eu metal can be detected by this principle.

Knowing the reference spectra, we analyze in detail the redox growth of EuO/$SrTiO_3$ at two exemplary temperatures, one being below the reevaporation temperature of the distillation process and one above that temperature. For the first 5 min of deposition at $T_P = 250\,^\circ$C mainly intensity from

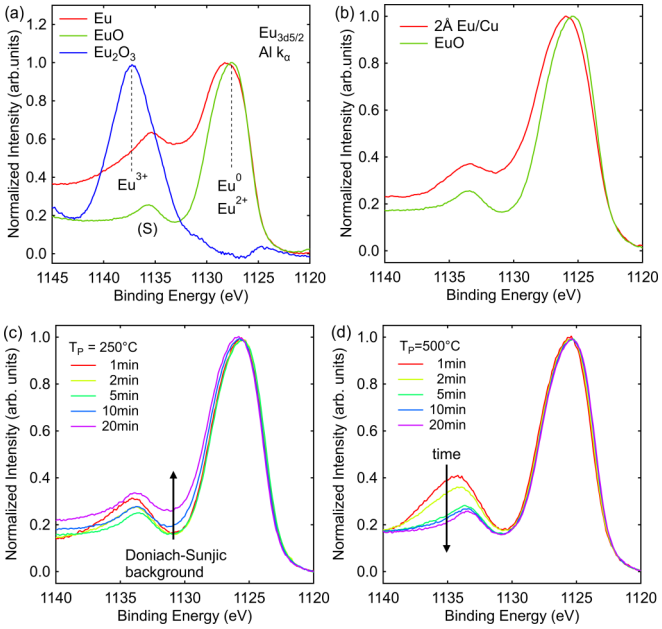

FIG. 1. Top: (a) Reference spectra of metallic, di- and trivalent Eu, EuO, and Eu_2O_3 films, respectively, obtained on the Eu $3d_{5/2}$ core level. (b) Comparison of stoichiometric EuO and $d \approx 2$ Å Eu metal on a metallic substrate. Bottom: XPS analysis of the Eu $3d_{5/2}$ for a stepwise EuO redox growth below (c) and above (d) the reevaporation temperature of Eu. For $t \geqslant 5$ min metal inclusions are observed, while at elevated temperature a decreasing Eu^{3+} content is present.

Eu^{2+} species are observed [Fig. 1(c)]. Less than 10% of Eu^{3+} is detected and the Eu^{3+} content reduces over time. However, for $t > 5$ min we observe Doniach-Sunjic inelastic background, indicating Eu metal inclusions in the film. Further deposition leads to an increase in background and indicates Eu^0. We conclude, that only a small amount of EuO is formed at this temperature for the initial growth. For extended growth the Eu metal inclusions turn the stoichiometry to Eu-rich.

Next, we study a stepwise Eu deposition at $T_P = 500\,^\circ$C [Fig. 1(d)]. For $t = 1$ min, we observe a spectrum with a mixture of Eu^{2+} (85%) and Eu^{3+} (15%) components, while contributions of Eu metal are absent. For continued growth the spectral weight from Eu^{3+} decreases (1% at $t = 20$ min). Already for $t > 5$ min, we find that the XPS spectra of adsorbed Eu metal are nearly indistinguishable from stoichiometric EuO reference data [compare Fig. 1(a)]. This demonstrates that the Eu metal is oxidized into a Eu^{2+}-rich (Eu^{2+}, Eu^{3+}) mixture at the $SrTiO_3$ interface. For extended growth only stoichiometric EuO (Eu^{2+}) is observed.

In the following, the stoichiometry of the grown film is quantified by fitting a linear combination of the reference spectra to the observed Eu $3d_{5/2}$ spectra. First, we discuss the Eu metal content of the grown films [Fig. 2(a)]. In addition to the findings presented for $T_P = 250\,^\circ$C, we find for $T_P \geqslant 350\,^\circ$C no Eu^0 metal in the spectra. We conclude that now Eu reevaporation is a dominant process, which is in line with previous reports utilizing the adsorption limited growth mode on YSZ [16].

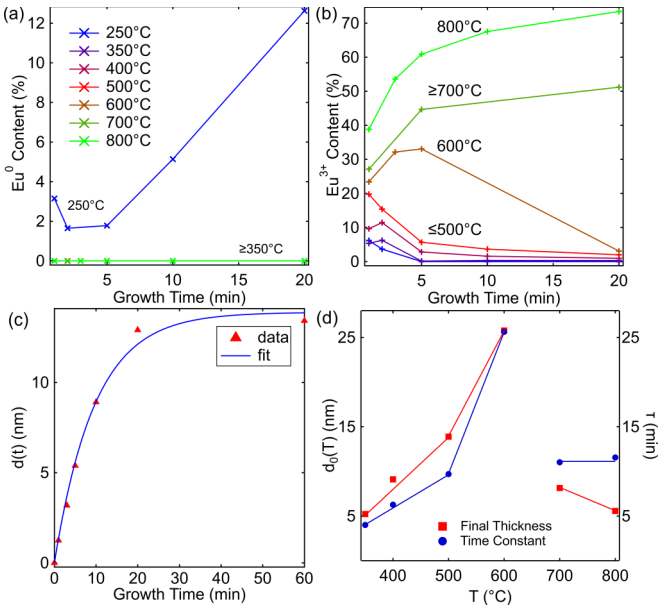

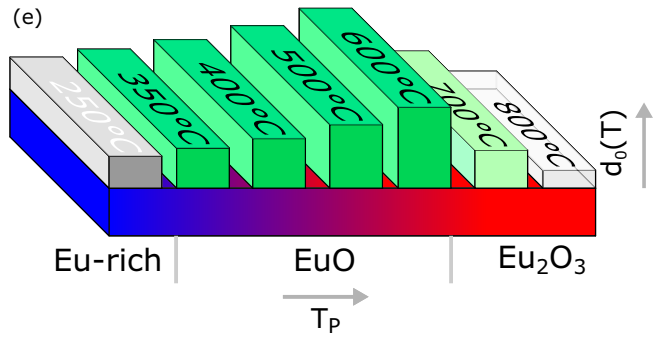

FIG. 2. Chemical quantification of the Eu $3d_{5/2}$ core level for metallic Eu^0 (a) and overoxidized Eu^{3+} (b) content as a function of t and T_P. (c) Exponential thickness dependence exemplary shown for a sample grown at $T_P = 500\,^\circ$C. (d) A reduction in d_0 and τ is observed at $t \geqslant 700\,^\circ$C at the same temperature where a Eu^{3+}-rich growth is observed. (e) We summarize the findings in a block diagram depicting the overall trend of the resulting film thickness and stoichiometry as a function of T_P.

We observe an exponential decay of the Eu^{3+} fraction with t for films prepared at $T_P = 250\,^\circ$C, $350\,^\circ$C, $400\,^\circ$C, and $500\,^\circ$C [Fig. 2(b)]. The Beer-Lambert law predicts an exponential decay of the intensity for the case of a buried layer with the growth overlayer thickness. Therefore, we argue that only the interface is responsible for the Eu^{3+} formation. It is also noted, that the Eu^{3+} content is higher at $t = 1$ min for increasing T_P. Yet, the total amount of Eu^{3+} is below one monolayer of Eu_2O_3, which is a negligible amount for extended film growth ($T_P = 500\,^\circ$C). For $T_P = 600\,^\circ$C, the Eu^{3+} content increases with t in the initial growth phase ($t \leqslant 5$ min). For the extended growth ($t \geqslant 5$ min) the content of Eu^{3+} decreases again and at $t = 20$ min only Eu^{2+} is found in the spectrum. Increasing the temperature further to $700\,^\circ$C, and $800\,^\circ$C, the content of Eu^{3+} increases monotonically with time and no EuO growth phase is observed. Therefore, redox growth for stoichiometric EuO on $SrTiO_3$ is possible only in the range $T_P = 350$–$600\,^\circ$C.

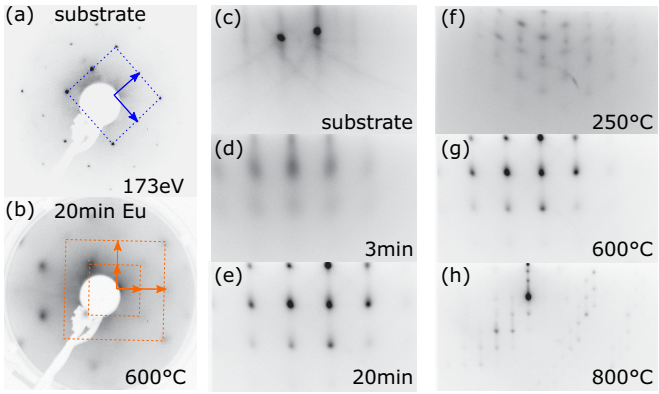

FIG. 3. *In situ* structure determination by LEED of the $SrTiO_3(001)$ substrate (a) and the redox-grown EuO film (b). We observe a 45° rotation of the EuO basis. (c)–(e) RHEED as a function of time shows a weak island growth mode and (f)–(h) structural transitions as a function of T_P from Eu^0 to Eu^{2+} and Eu^{3+}, respectively. The RHEED beam is parallel to $SrTiO_3(110)$ using 20 keV electrons.

A. Thickness dependence

Exemplary shown for a sample grown at $T = 500\,^\circ$C, we find the temporal dependence of the thickness, $d(t)$ (see Supplemental Material [21]), to follow an exponential law of the form $d(t) = d_0[1 - \exp(-t/\tau)]$ [Fig. 2(c)]. Here d_0 is the final thickness and τ is the time constant. We apply this model to all samples [Fig. 2(d)] and find that both d_0 and τ increase monotonically for $T \leqslant 600\,^\circ$C. Above this temperature a significant reduction is observed for both d_0 and τ, simultaneous to the transition to Eu^{3+}-rich growth as observed in the chemical analysis.

We find that EuO-rich films (i.e., $350\,^\circ\text{C} \leqslant T_P \leqslant 600\,^\circ$C) can be grown with up to $d = 25$ nm and $\tau = 25$ min. The fact that the time constants are in the range of many minutes allows a precise control of the film thickness by stopping the growth at a suitable time. The resulting chemical composition and thickness are compiled in a block diagram as a function of temperature [Fig. 2(e)].

B. Structural profile

For the *in situ* stuctural analysis we first present LEED [Fig. 3(a)] for the $SrTiO_3$ substrate. We observe clear and sharp reflexes. The LEED pattern is fourfold symmetric, reflecting the symmetry of the perovskite lattice. Indicated by blue arrows is the basis of the reciprocal lattice. The EuO film [$T_P = 600\,^\circ$C, Fig. 3(b)] is well ordered and exhibits LEED reflexes, with a basis rotated by 45° to that of $SrTiO_3$; the epitaxial relationship is $EuO(110)/SrTiO_3(100)$. The LEED reflexes are wider indicating a small degree of mosaicity.

In Figs. 3(c)–3(e) we show RHEED of the substrate and Eu deposition for $t = 3$min and $t = 20$min at $T_P = 600\,^\circ$C. The substrate shows RHEED streaks and two sharp spots on the Laue circle, indicating a flat and well-oriented substrate. At 3 min Eu deposition we observe RHEED streaks and a weak transmission pattern. For continued growth the transmission pattern dominates the RHEED reflexes, indicating an island type growth mode.

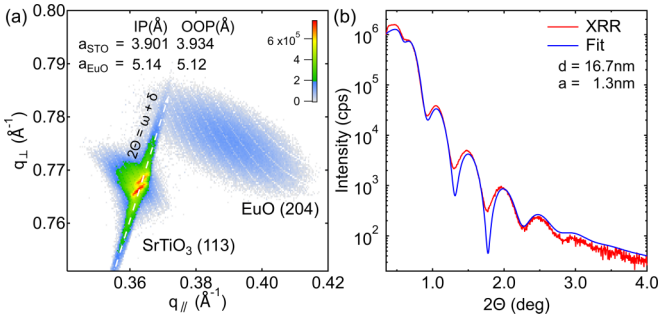

FIG. 4. *Ex situ* x-ray analysis of a sample grown at 600 °C. The reciprocal space map (a) shows the $SrTiO_3$(113) and EuO(204) peak in close proximity, a consequence of the epitaxial relation of EuO(110)/$SrTiO_3$(100). The x-ray reflectometry shows that the film has a low roughness of 1.32 nm (b).

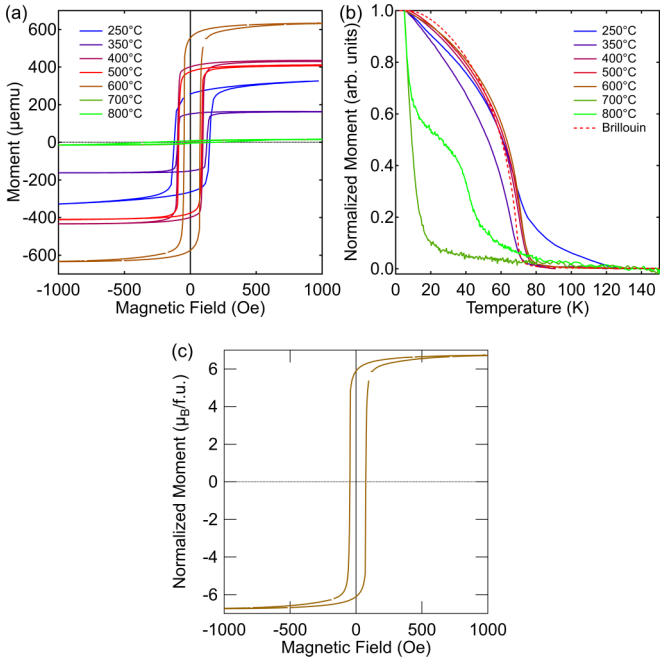

FIG. 5. Magnetic properties of a temperature series of redox-grown Eu-oxide thin films on $SrTiO_3$ as (a) a function of applied magnetic field and (b) temperature. EuO-rich films, as found in the chemical analysis, exhibit a hysteresis, while high Eu^{3+} contents lead to paramagnetism. The inclusion of Eu^0 as seen at $T_P = 250$ °C causes a magnetic tail in the temperature dependence. The normalized magnetic moment hysteresis (c) shows M_S close to the bulk value of pure EuO ($T_P = 600$ °C).

The RHEED reflexes as a function of T_P = (250, 600, and 800) °C are shown in Figs. 3(f)–3(h). For Eu-rich growth at 250 °C we observe the hexagonal RHEED reflexes of the Eu-metal crystal. At elevated temperature the expected EuO-related reflexes dominate the RHEED pattern, as described above. Finally at $T_P = 800$ °C the structure shows the much bigger unit cell, and therefore shorter distances between RHEED reflexes, of the cubic Eu_2O_3 crystal and a complex transmission pattern.

In conclusion, we observe clear structural transitions that are perfectly in line with the results from the chemical analysis by XPS. The EuO films grow by a redox-driven process epitaxially and are, except for a small surface roughness, flat.

In Fig. 4(a), we show the *ex situ* x-ray analysis, starting with a RSM of a sample grown at $T_P = 600$ °C. The Bragg peaks from the $SrTiO_3$(113) and the EuO(204) peak are shown. The simultaneous observation of both reflexes is in line with the expected rotation of both lattices EuO(110) ∥ $SrTiO_3$(100), since the reflexes would otherwise be observed at an angle of 45 °. The EuO(204) reflex has a rocking curve width of $\delta\omega = 1.1°$ in line with the widened LEED reflexes. We calculate the lattice parameters for the in-plane and out-of-plane lattice constants and find that both $SrTiO_3$ and EuO ($a_{SrTiO_3} = 3.901$ Å and $a_{EuO} = 5.14$ Å) are close to the literature values ($a_{SrTiO_3} = 3.905$ Å and $a_{EuO} = 5.14$ Å [24]).

In Fig. 4(b), we depict the corresponding XRR curve and a fit to the measured data points using the Parrat formalism. The grown film exhibits a total thickness of $d = 16.7$ nm, while the roughness is $a = 1.3$ nm. Hence we conclude that the redox-growth process produces well-oriented, i.e., 45° rotated, EuO films on $SrTiO_3$ with a small degree of roughness.

C. Magnetic properties

The magnetic properties of samples grown at $T_P = 250$–800 °C are depicted in Fig. 5(a) as hysteresis loops and as a function of temperature $M(T)$ in Fig. 5(b). The hysteresis loops are shown in absolute values, allowing a direct comparison of the total moment of the grown film. Since EuO is the only ferromagnetic component in the stack, it is expected that the saturation magnetization M_S is proportional to the EuO thickness. Eu metal and Eu_2O_3 exhibit small paramagnetic moments only. In the chemical analysis we showed that the EuO content and the thickness both depend on T_P in a complex manner. Consequently, the magnetic analysis cannot be expected to follow a simple linear temperature dependence.

All $M(H)$ curves of T_P = (350, 400, 500, and 600)°C increase monotonically in M_S, while the coercive field, H_C, decreases simultaneously. Unordered and thin films are generally considered to cause an increase of the coercive field [25]. This finding suggest, that the amount of ferromagnetic EuO increases as a function of the temperature and forms a more ordered lattice at higher temperatures.

The samples grown at T_P = (700 and 800) °C exhibit no hysteresis, which is in line with the chemical analysis that reveals a Eu_2O_3-rich (and therefore paramagnetic) composition.

The temperature dependence of the normalized magnetic moment is shown in Fig. 5(b). We find for the samples grown at $T_P = 350$–600 °C a Brillouin-like shape that closely follows a simulation with a Curie temperature of $T_C = 69$ K, the literature value for EuO [26]. Significant deviations are observed for samples grown at high temperature, where a paramagnetic behavior is measured and for $T_P = 250$ °C, where a pronounced metallic tail indicates the presence of Eu-metal ions included in a EuO film [27,28].

In Fig. 5(c) we depict the normalized hysteresis curve of one film grown at $T_P = 600$ °C. The saturation moment of $M_S = 6.73 \pm 0.03(\text{stat}) \pm 0.33(\text{sys})\mu_B$/f.u. is close to the bulk expectation. Due to optically determining the surface area a systematic error of 5% has to be expected using this method.

IV. DISCUSSION

Unlike the classical EuO synthesis processes—for which oxygen gas is supplied during a reactive molecular beam epitaxy growth process—here the oxide substrate itself acts as the supplier of oxygen: The $SrTiO_3$ substrate is reduced by the presence of Eu while the reactant oxidizes to EuO, Eu_3O_4, or Eu_2O_3. These processes can be assessed with an Ellingham analysis (see Supplemental Material [21]). Indeed, we find that at equilibrium the most likely formed oxide is Eu_2O_3. However, we observe the formation of EuO in the intermediate temperature range. We therefore describe the complex redox growth of $EuO/SrTiO_3$ as an interplay of three factors: (i) the kinetics of the oxygen anion reservoir from the substrate, (ii) the kinetics of the Eu metal on the surface of $SrTiO_3$ (and its concomitant reevaporation), and (iii) the thermodynamics of the interface reactions.

As seen in Fig. 2(c) the thickness of a redox-grown Eu oxide film is limited. This is surprising, as a normal diffusion type growth would have led to a $d \propto \sqrt{t}$ type behavior [29,30]. We explain the thickness limit as a consequence of the insulating properties of the Eu oxides: The O^{2-} ions are charged and have to cross an insulating film of already grown Eu oxides. This is well described in the context of a Mott-Cabrera type growth mode as was also found for the oxidation of Fe [31,32]. In the Mott-Cabrera type growth, the potential that the O^{2-} ion is submitted to depends on the thickness of the film and its ion-related resistivity. This explains the sudden reduction of d_0 and τ at the transition to Eu^{3+} rich growth in Fig. 2(d), as the resistance is larger for the higher Eu oxides. Also, the reevaporation of Eu from the surface can be expected to be much faster.

V. OUTLOOK

In order to explore the redox-driven growth of EuO more generally, we study the initial growth ($t = 5$ min) at elevated temperatures ($T_P = 500\,^{\circ}$C) of Eu(O) on YSZ, $(LaAlO_3)0.3(Sr_2TaAlO_6)0.7$ (LSAT), 10 nm SrO grown on $SrTiO_3$, $LaAlO_3$ (LAO), and MgO and compare it to the previous results of $SrTiO_3$.

Again we study the Eu $3d_{5/2}$ core level, as shown in Fig. 6(a). In the case for MgO and LAO we observe Eu^0 in the film even at this high T_P. For SrO and LSAT, we observe only Eu^{2+}, whereas for MgO and YSZ we even observe some Eu^{3+}. This is surprising, as preparations on YSZ are often reported in adsorption-limited growth conditions and the interfacial oveoxidation is not mentioned [14].

We obtain the film thickness, d (see Supplemental Material) for all redox-grown films and compare them to estimates for the ionic conductivities of the respective oxide substrate [33–38]. We find that d qualitatively scales with the ionic conductivities of the underlying substrate [Fig. 6(b)]. We attribute the high discrepancy between SrO conductivity and d of redox-grown EuO to the fact that the SrO thin film grown on a $SrTiO_3$ will have a higher oxygen mobility than a bulk crystal, due to crystal defects.

From this analysis we are able to differentiate substrates into active substrates, with a relevant redox process and passive substrates, where additional oxygen needs to be supplied.

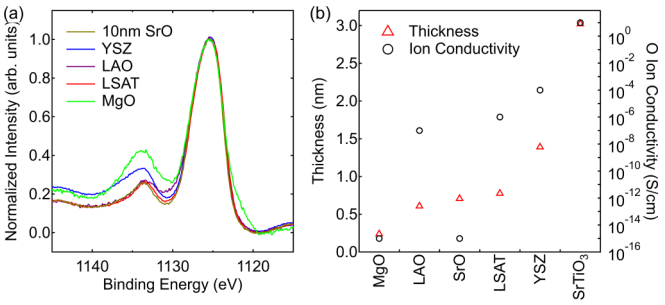

FIG. 6. (a) XPS analysis of the Eu $3d_{5/2}$ core level for redox-grown Eu oxides; (b) calculated thickness d and oxygen ion conductivity σ for a selection of oxides grown at $T_P = 500\,^{\circ}$C and $t = 5$ min. A qualitative correlation between d and σ is observed.

We find that $SrTiO_3$ is the most active substrate for redox growth. LAO, SrO thin films, LSAT, and YSZ might pose as suitable templates for thin films and are expected to lead to thinner EuO overlayers than would be expected for $SrTiO_3$, while MgO and LAO act as passive substrates.

VI. CONCLUSIONS

In summary, we report a novel route for the synthesis of stoichiometric and single-crystalline EuO films without supplying gaseous oxygen. Instead, utilizing the oxidic substrate as a source of oxygen is the key to a reliable and simplified preparation scheme. We have identified the parameter window in which EuO can be grown on $SrTiO_3(001)$ and reduce the complexity of the typically applied distillation growth mode.

The prepared films show the expected chemical, structural, and magnetic properties of stoichiometric EuO in the temperature range $T_P = 350$–$600\,^{\circ}$C. By changing the growth temperature, the total thickness of the EuO film can be varied from 9 to 25 nm for $t = 60$ min, and by stopping the growth earlier the thickness can be varied freely. Thus the redox-driven EuO growth method allows one to prepare thicker films compared to a topotactic synthesis mechanism. All redox-grown EuO films grown in the suitable parameter window exhibit bulk ferromagnetic properties with no metal inclusions. With regard to the structural properties, we have observed flat and well-oriented films with the epitaxial relationship of $EuO(110) \parallel SrTiO_3(100)$.

Finally, we demonstrate that the redox-driven EuO growth scheme can be successfully applied not only to $SrTiO_3$, but also to other oxide substrates. We believe, that the universality of a redox-controlled oxide thin-film synthesis may also open up exciting perspectives for other topical oxide materials and their integration into complex oxide heterostructures.

ACKNOWLEDGMENTS

We thank David N. Müller for fruitful discussions about solid-state oxide chemistry. We thank O. Petracic and the Jülich Centre for Neutron Science for providing measurement time at the magnetometers. M.M. acknowledges financial support from Helmholtz Association under Contract No. VH-NG-811.

[1] H. Y. Hwang, Y. Iwasa, M. Kawasaki, B. Keimer, N. Nagaosa, and Y. Tokura, Emergent phenomena at oxide interfaces, Nat. Mater. **11**, 103 (2012).

[2] M. Lorenz, M. S. Ramachandra Rao, T. Venkatesan, E. Fortunato, P. Barquinha, R. Branquinho, D. Salgueiro, R. Martins, E. Carlos, A. Liu, F. K. Shan, M. Grundmann, H. Boschker, J. Mukherjee, M. Priyadarshini, N. DasGupta, D. J. Rogers, F. H. Teherani, E. V. Sandana, P. Bove, K. Rietwyk, A. Zaban, A. Veziridis, A. Weidenkaff, M. Muralidhar, M. Murakami, S. Abel, J. Fompeyrine, J. Zuniga-Perez, R. Ramesh, N. A. Spaldin, S. Ostanin, V. Borisov, I. Mertig, V. Lazenka, G. Srinivasan, W. Prellier, M. Uchida, M. Kawasaki, R. Pentcheva, P. Gegenwart, F. Miletto Granozio, J. Fontcuberta, and N. Pryds, The 2016 oxide electronic materials and oxide interfaces roadmap, J. Phys. Appl. Phys. **49**, 433001 (2016).

[3] D. C. Vaz, A. Barthélémy, and M. Bibes, Oxide spin-orbitronics: New routes towards low-power electrical control of magnetization in oxide heterostructures, Jpn. J. Appl. Phys. **57**, 0902A4 (2018).

[4] M. Uchida and M. Kawasaki, Topological properties and functionalities in oxide thin films and interfaces, J. Phys. Appl. Phys. **51**, 143001 (2018).

[5] H. Huang, Y. Xu, J. Wang, and W. Duan, Emerging topological states in quasi-two-dimensional materials: Emerging topological states in quasi-2D materials, Wiley Interdiscip. Rev. Comput. Mol. Sci. **7**, e1296 (2017).

[6] M. Müller, G.-X. Miao, and J. S. Moodera, Exchange splitting and bias-dependent transport in EuO spin filter tunnel barriers, Europhys. Lett. **88**, 47006 (2009).

[7] A. Mauger and C. Godart, The magnetic, optical, and transport properties of representatives of a class of magnetic semiconductors: The europium chalcogenides, Phys. Rep. **141**, 51 (1986).

[8] G. M. Prinz, T. Gerber, A. Lorke, and M. Müller, Quantum confinement in EuO heterostructures, Appl. Phys. Lett. **109**, 202401 (2016).

[9] P. Lömker, T. C. Rödel, T. Gerber, F. Fortuna, E. Frantzeskakis, P. Le Fèvre, F. Bertran, M. Müller, and A. F. Santander-Syro, Two-dimensional electron system at the magnetically tunable $EuO/SrTiO_3$ interface, Phys. Rev. Mater. **1**, 062001(R) (2017).

[10] T. C. Rödel, F. Fortuna, S. Sengupta, E. Frantzeskakis, P. L. Fèvre, F. Bertran, B. Mercey, S. Matzen, G. Agnus, T. Maroutian, P. Lecoeur, and A. F. Santander-Syro, Universal fabrication of 2D electron systems in functional oxides, Adv. Mater. **28**, 1976 (2016).

[11] E. Lesne, Y. Fu, S. Oyarzun, J. C. Rojas-Sánchez, D. C. Vaz, H. Naganuma, G. Sicoli, J.-P. Attané, M. Jamet, E. Jacquet, J.-M. George, A. Barthélémy, H. Jaffrès, A. Fert, M. Bibes, and L. Vila, Highly efficient and tunable spin-to-charge conversion through Rashba coupling at oxide interfaces, Nat. Mater. **15**, 1261 (2016).

[12] Q. Song and H. Zhang, Observation of inverse Edelstein effect in Rashba-split 2DEG between $SrTiO_3$ and $LaAlO_3$ at room temperature, Sci. Adv. **3**, e1602312 (2017).

[13] M. Bibes, N. Reyren, E. Lesne, J.-M. George, C. Deranlot, S. Collin, A. Barthelemy, and H. Jaffres, Towards electrical spin injection into $LaAlO_3$-$SrTiO_3$, Philos. Trans. R. Soc., A **370**, 4958 (2012).

[14] R. Sutarto, S. G. Altendorf, B. Coloru, M. Moretti Sala, T. Haupricht, C. F. Chang, Z. Hu, C. Schüßler-Langeheine, N. Hollmann, H. Kierspel, H. H. Hsieh, H.-J. Lin, C. T. Chen, and L. H. Tjeng, Epitaxial and layer-by-layer growth of EuO thin films on yttria-stabilized cubic zirconia (001) using MBE distillation, Phys. Rev. B **79**, 205318 (2009).

[15] T. Gerber, P. Lömker, B. Zijlstra, C. Besson, D. N. Mueller, W. Zander, J. Schubert, M. Gorgoi, and M. Müller, Thermodynamic stability and control of oxygen reactivity at functional oxide interfaces: EuO on ITO, J. Mater. Chem. C **4**, 1813 (2016).

[16] P. Steeneken, New light on EuO thin films, Ph.D. thesis, Rijksuniversiteit Groningen, 2002.

[17] R. W. Ulbricht, A. Schmehl, T. Heeg, J. Schubert, and D. G. Schlom, Adsorption-controlled growth of EuO by molecular-beam epitaxy, Appl. Phys. Lett. **93**, 102105 (2008).

[18] T. Mairoser, J. A. Mundy, A. Melville, D. Hodash, P. Cueva, R. Held, A. Glavic, J. Schubert, D. A. Muller, D. G. Schlom, and A. Schmehl, High-quality EuO thin films the easy way via topotactic transformation, Nat. Commun. **6**, 7716 (2015).

[19] H. Miyazaki, H. Momiyama, T. Hajiri, T. Ito, K. Imura, M. Matsunami, and S. Kimura, Fabrication of single crystalline EuO thin film with SrO buffer layer on $SrTiO_3$ substrate, J. Phys. Conf. Ser. **391**, 012047 (2012).

[20] N. Iwata, G. Pindoria, T. Morishita, and K. Kohn, Preparation and magnetic properties of EuO thin films epitaxially grown on MgO and $SrTiO_3$ ubstrates, J. Phys. Soc. Jpn. **69**, 230 (2000).

[21] See Supplemental Material at http://link.aps.org/supplemental/10.1103/PhysRevMaterials.3.061401 for description of substrate preparation, *ex situ* characterization, thermodynamical analysis, and considerations of the thickness determination.

[22] C. Caspers, M. Müller, A. X. Gray, A. M. Kaiser, A. Gloskovskii, C. S. Fadley, W. Drube, and C. M. Schneider, Chemical stability of the magnetic oxide EuO directly on silicon observed by hard x-ray photoemission spectroscopy, Phys. Rev. B **84**, 205217 (2011).

[23] E.-J. Cho, S.-J. Oh, S. Imada, S. Suga, T. Suzuki, and T. Kasuya, Origin of the high-binding-energy structure in the 3*d* core-level spectra of divalent Eu compounds, Phys. Rev. B **51**, 10146 (1995).

[24] G. Bergerhoff and I. D. Brown, Inorganic crystal structure database, in *Crystallographic Databases*, edited by F. H. Allen, G. Bergerhoff, and R. Sievers (International Union of Crystallography, Bonn/Cambridge/Chester, 2017), pp. 77–95.

[25] M. Müller, G.-X. Miao, and J. S. Moodera, Thickness dependence of ferromagnetic- and metal-insulator transition in thin EuO films, J. Appl. Phys. **105**, 07C917 (2009).

[26] B. T. Matthias, R. M. Bozorth, and J. H. Van Vleck, Ferromagnetic Interaction in EuO, Phys. Rev. Lett. **7**, 160 (1961).

[27] J. C. Suits, K. Lee, H. F. Winters, P. B. P. Phipps, and D. F. Kyser, Annealing study of EuO films doped with iron and europium, J. Appl. Phys. **42**, 1777 (1971).

[28] S. G. Altendorf, A. Efimenko, V. Oliana, H. Kierspel, A. D. Rata, and L. H. Tjeng, Oxygen off-stoichiometry and phase separation in EuO thin films, Phys. Rev. B **84**, 155442 (2011).

[29] A. Einstein, Über die von der molekularkinetischen theorie der wärme geforderte bewegung von in ruhenden flüssigkeiten suspendierten teilchen, Ann. Phys. **322**, 549 (1905).

[30] R. A. De Souza, Oxygen diffusion in $SrTiO_3$ and related perovskite oxides, Adv. Funct. Mater. **25**, 6326 (2015).

[31] N. Cabrera and N. F. Mott, Theory of the oxidation of metals, Rep. Prog. Phys. **12**, 163 (1949).

[32] J. Kruger and H. T. Yolken, Room temperature oxidation of iron at low pressures, CORROSION **20**, 29t (1964).

[33] S. J. Skinner and J. A. Kilner, Oxygen ion conductors, Mater. Today **6**, 30 (2003).

[34] F. Gunkel, P. Brinks, S. Hoffmann-Eifert, R. Dittmann, M. Huijben, J. E. Kleibeuker, G. Koster, G. Rijnders, and R. Waser, Influence of charge compensation mechanisms on the sheet electron density at conducting $LaAlO_3/SrTiO_3$-interfaces, Appl. Phys. Lett. **100**, 052103 (2012).

[35] J. Rudolph, Über den leitungsmechanismus oxydischer halbleiter bei hohen temperaturen, Z. Naturforsch. A, Phys. Sci. **14**, 727 (1959).

[36] T. Nguyen, The effect of oxygen vacancy on the oxide ion mobility in $LaAlO_3$-based oxides, Solid State Ionics **130**, 229 (2000).

[37] S. P. Mitoff, Electronic and ionic conductivity in single crystals of MgO, J. Chem. Phys. **36**, 1383 (1962).

[38] R. Moos and K. H. Hardtl, Defect chemistry of donor-doped and undoped strontium titanate ceramics between 1000 and 1400, J. Am. Ceram. Soc. **80**, 2549 (2005).